LASER INTERFEROMETER GRAVITATIONAL WAVE OBSERVATORY
- LIGO -
CALIFORNIA INSTITUTE OF TECHNOLOGY
MASSACHUSETTS INSTITUTE OF TECHNOLOGY

Technical Note **LIGO-T1400334–vX** 2014/08/06

Thermal Noise Reduction in Coating-Less Optical Cavities

Sam Moore

California Institute of Technology
LIGO Project, MS 18-34
Pasadena, CA 91125
Phone (626) 395-2129
Fax (626) 304-9834
E-mail: info@ligo.caltech.edu

Massachusetts Institute of Technology
LIGO Project, Room NW22-295
Cambridge, MA 02139
Phone (617) 253-4824
Fax (617) 253-7014
E-mail: info@ligo.mit.edu

LIGO Hanford Observatory
Route 10, Mile Marker 2
Richland, WA 99352
Phone (509) 372-8106
Fax (509) 372-8137
E-mail: info@ligo.caltech.edu

LIGO Livingston Observatory
19100 LIGO Lane
Livingston, LA 70754
Phone (225) 686-3100
Fax (225) 686-7189
E-mail: info@ligo.caltech.edu

http://www.ligo.caltech.edu/

Abstract

Lasers need to have low frequency and phase noise when used in high-precision measurements (such as gravitational wave detection). The overall aim of this project is to reduce the frequency and phase noise specific to temperature fluctuations in an optical cavity. There are two forms of thermal noise, namely thermoelastic noise (associated with length fluctuations) and thermorefractive noise (associated with index of refraction fluctuations). Our optical cavity is a rectangular block, utilizing total internal reflection. Analytical and Finite element thermorefractive thermal noise calculations are presented here for this cavity. In the future these thermal noise calculations will be used to find a material that minimizes the total thermal noise. Faster methods are employed for calculating this thermal noise: the heat equation is solved using a steady-state, transient free ansatz. Moreover, we are searching for the best mesh distribution that solves the problem quickly and accurately.

1 Motivation

Laser frequency stabilization is important for use in high-precision measurements (such as gravitational wave detection). The cavity from which the laser originates contains many sources of noise, such as thermal and mechanical fluctuations [3]. To achieve the precision necessary for gravitational wave detection, this project aims to reduce noise in these cavities. Optical cavities often contain highly reflective coatings, which have the problem of high mechanical (Brownian) noise. As a result, this project removes the reflective coatings in the resonator and instead uses total internal reflection. The goal will then be to minimize the thermal noise associated with this cavity.

2 TIR Cavity

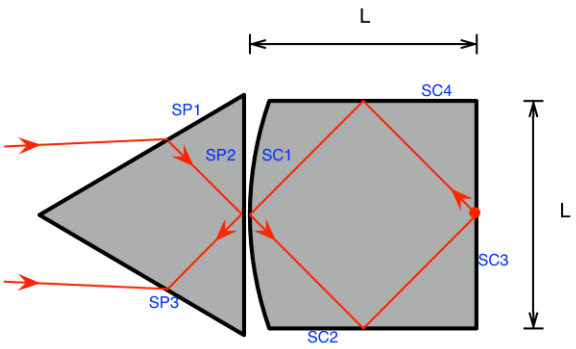

Figure 1: Our total internal reflection cavity. A prism and cavity are separated a distance on the order of the wavelength of the laser light. When the light enters the prism, an evanescent part of the light enters the cavity (a process called frustrated total internal reflection).

Our optical cavity removes all of the multilayer coatings that are usually present. In doing

so, losses upon reflection are reduced; as mentioned previously, Brownian noise is prevalent in multilayer coatings. The cavity operates by using total internal reflection (TIR). For this to work, it must be that $n_2 < n_1$ [1], where n_1 is the index of refraction of the cavity, and n_2 is the index of refraction of the surrounding medium.

Furthermore, the angle of incidence θ inside of the medium n_1 must satisfy $\sin\theta > n_2/n_1$ for TIR to occur. This means that the values by which n_1 and n_2 differ depends on the geometry of the cavity. For example, if we describe total internal reflection inside of a square, $\theta = 45°$, so $n_1/n_2 > 1.41$. For a triangle, meanwhile, $n_1/n_2 > 2$.

How does the light first get into and out of the cavity? It "leaks" into the cavity by use of frustrated total internal reflection. Here, another material is placed a distance of order λ (light wavelength) from the cavity. This allows an evanescent wave to travel into and out of the cavity.

3 Thermal Noise

Gravitational wave interferometers deal with many sources of noise, which is why it is important to have a strong signal. The arms of the interferometer contain optical cavity "test masses," which are used to amplify the laser beam signal. For this optical cavity, thermal noise is the most relevant, and this project seeks to minimize this thermal noise. There are three sources of thermal noise: Brownian noise, Thermoelastic (TE) noise, and Thermorefractive (TR) noise.

3.1 Fluctuation Dissipation Theorem

The Fluctuation Dissipation theorem (FDT) will be the primary tool used to calculate the thermal noise. The central idea of the FDT is that fluctuations cause dissipation. Hence, if we have low fluctuations, there will also be low dissipation. Notice that this is relating a microscopic property to a macroscopic property. The dissipation (a macroscopic property) is usually the observed property, which means that it can be used to infer the thermal fluctuations.

3.2 Levin's Approach

Levin's approach utilizes the FDT to calculate thermal noise. The technique works for non-uniform dissipation and an arbitrary laser beam size. To calculate the thermal noise $S_z(f)$ at a frequency f, one applies an oscillatory generalized force $F_0\cos(2\pi ft)f(\vec{r})$ to the geometry of interest (the "test mass") [4]. $f(\vec{r})$ indicates the shape of the laser beam on the surface of that geometry. In this process, one can calculate W_{diss}, the dissipation associated with the friction of the test mass. In the Levin paper, $S_z(f)$ can then be calculated via

$$S_z(\omega) = \frac{8k_BT}{\omega^2}\frac{W_{\text{diss}}}{F_0^2} \tag{1}$$

where T is the temperature of the test mass. Note that the F_0 term is not necessary to calculate because it cancels out with the F_0 in the expression for W_{diss}.

3.3 Brownian Noise

We have previously mentioned Brownian Noise when discussing reflective coatings. This is an effect that arises out of Brownian motion, where particles in a fluid are observed to jostle randomly while suspended in a fluid. It was first discovered in 1828, but remained a mystery until Einstein, in 1905, used the finding to demonstrate the existence of atoms. Brownian motion can be described using the Diffusion equation, where particles move from high to low concentrations. Brownian noise manifests itself as slight, fluctuating distortions in the shape of the cavity. Brownian noise can occur in an optical cavity's reflectors, and is especially prevalent in multilayer mirror coatings.

3.4 Thermorefractive Noise

The second source source of noise is thermorefractive (TR) noise, caused by fluctuations in the index of refraction of the cavity. The result of these fluctuations is that radiation in the cavity develops random fluctuations in its phase. The parameter $\beta \equiv \frac{\partial n}{\partial T}$ characterizes this TR noise (where n is the index of refraction). For Thermorefractive noise (see description below), the generalized force of the Levin Approach has the form of an oscillatory heat source [5]:

$$q(\vec{r}, t) = T(\vec{r}, t) F_0 \cos(2\pi f t) f(\vec{r}) \tag{2}$$

where $T(\vec{r}, t)$ describes the temperature distribution at a point $\vec{r}$ and time t. $f(\vec{r})$ describes the shape of the laser beam as it propagates through the cavity. Given the heat source in equation 2, one can solve for the temperature distribution via the heat equation:

$$C_p \frac{\partial T}{\partial t} - \kappa \nabla^2 T = \dot{q}(\vec{r}, t), \tag{3}$$

where C_p is the heat capacity per volume at constant pressure and κ is the thermal conductivity. Now, temperature *gradients* are the true quantities of interest because they cause heat flux—and therefore energy dissipation—in the test mass. The dissipation is related to the temperature gradient via

$$W_{\text{diss}} = \frac{1}{2T_0} \int_V \kappa |\nabla T|^2 \, dV \tag{4}$$

where κ is the thermal conductivity and T_0 is a homogeneous reference temperature of the test mass. From this, one can use the FDT (eq. 1) to calculate the thermal noise.

In last year's approach, the TR noise was calculated by solving for the time-dependent solution $T(\vec{r}, t)$ (eq. 3). Here, the goal is a less computationally expensive approach. We assume a steady-state temperature $T(\vec{r}, t) = T(\vec{r}) e^{i\omega t}$, given a heat injection $q(\vec{r}, t) = q(\vec{r}) e^{i\omega t}$, which yields a stationary differential equation of the form

$$i\omega C_p T(\vec{r}) - \kappa \nabla^2 T(\vec{r}) = i\omega q(\vec{r}) \tag{5}$$

With this method, one can use eq. 4 without dealing with transient temperature distributions.

3.5 Thermoelastic Noise

The third source of noise is thermoelastic (TE) noise, which arises from thermal fluctuations in a cavity's mirror and optical coatings. These thermal fluctuations cause the cavity to create small, fluctuating deformations throughout its surface. These geometry changes then cause fluctuations (i.e. noise) in the laser's frequency. TE noise is characterized by an expansion coefficient α.

3.6 Thermo-optic Noise

TE and TR noise can be combined together, which is the aim of this project. Evans et. al [2] showed that in a cavity with multilayer coatings, the TE and TR mechanisms have a negative relative sign in the overall thermal noise ("thermo-optic" noise) spectrum, leading to possible thermal noise cancellation. However, this relative negative sign does not occur with coating-less cavities. As a result, last year's project sought materials whose parameters α and β *themselves* had a relative sign difference (as opposed to a sign difference in the power spectrum) [3].

Since TE and TR noise both derive from the same source—thermal fluctuations—it is reasonable to suspect correlation between the two noise sources. Indeed, last year's project found that TE and TR noise are at least somewhat correlated. The more correlated these sources are, the more cancellation between α and β is possible. A long-term goal of this project is to determine this noise correlation.

4 Finite Element Analysis (Progress so Far)

COMSOL and MATLAB are being used to simulate the sources of noise. The COMSOL model utilizes Finite element analysis and the Fluctuation Dissipation theorem.

4.1 Test Cases

Progress has been made in verifying the COMSOL model for TR noise in cylindrical test masses, as presented in Heinert et al [5]. Here, the aim is to calculate the TR noise in a cylinder subject to adiabatic boundary conditions ($\nabla T = 0$ at the boundary). Heinert et al. derives a plot for this TR noise $\sqrt{S_z(f)}$, where f is the frequency of a heat injection, following Levin's approach. The heat injection is assumed to be of the form of equation 2. If one further assumes small temperature fluctuations, $T(\vec{r}, t)$ in equation 2 can be taken as a constant ambient temperature T_0.

We a assume the laser is a Gaussian beam. Hence, for the cylindrical test mass, we have that $f(\vec{r}) = \frac{\beta}{\pi r_0^2} e^{-r^2/r_0^2}$, where r is the distance from the center of the cylinder, and r_0 is the beam radius. We can therefore write $q(\vec{r}) = Ae^{-r^2/r_0^2}$, where $A \equiv \beta T_0 F_0/(\pi r_0^2)$. Once COMSOL calculates the temperature profile, the dissipation is calculated via equation (3), and the TR noise is calculated via equation (1). Heinert's paper derives a TR displacement

noise expression of

$$S_z(\omega) = \frac{16}{\pi} k_B T_0^2 \frac{H\kappa\beta^2}{r_0^4 C_p^2} \times \sum_{n=1}^{\infty} \frac{a_n^2}{[J_0(a_n)]^2} \frac{K_n^2}{\omega^2 + \frac{\kappa^2 a_n^4}{C_p^2 R^4}} \tag{6}$$

where $J_0(x)$ is the zeroth order bessel function of the first kind, R is the radius of the cylinder, H is the height, a_n is a zero of $J_1(x)$, and

$$K_n = \int_0^1 J_0(a_n \rho) e^{-((R/r_0)\rho)^2} \rho \, d\rho \tag{7}$$

The following noise plot in figure 2 was obtained for a silicon test mass at $T_0 = 10$ K. The solid line represents the analytical calculation, eq. 6, while the dots represent COMSOL's calculations. Two COMSOL models were used: a 1D axisymmetric model, and a full-scale 3D cylindrical model. Both gave close to the same result.

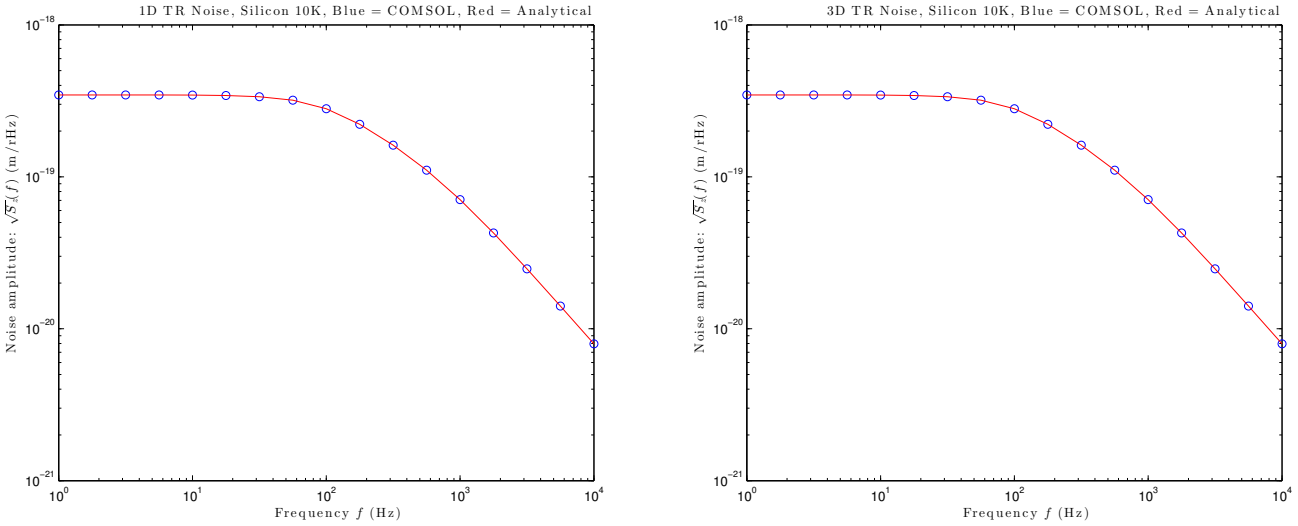

Figure 2: Displacement TR noise as a function of frequency f for silicon at 10 K. The verification is shown for two different types of models in COMSOL. The 3D model (right) is the most general model, and it still runs much faster than the previous time-dependent model.

Figure 2 shows that a 1D axisymmetric model (left) and a full 3D model (right) in COMSOL both yield agreement with the red analytical curve (eq. 6). It should also be emphasized that the steady-state temperature approach in eq. 5 allowed these plots to be generated much faster than before.

The next step was to provide a similar verification for TE noise, using the same steady-state method as before. For these calculations, we referred to the Duan paper [6]. Duan calculates thermo-optic noise (referred to as "thermoconductive" noise in the paper) of a cylinder of height H and radius R using a different analytical approach than Heinert et al. The calculation is of the thermoconductive phase noise

$$S_\phi(f) = \frac{4\pi^2}{\lambda^2} H^2 (\beta + n\alpha)^2 S_{\delta T}(f), \tag{8}$$

where $S_T(f)$ is the noise associated with thermal fluctuations, and is related to thermo-optic displacement noise via $S_z(f) = H^2(\beta + n\alpha)^2 S_T(f)$. (One also needs to divide Heinert's expression by 4π to match Duan's Fourier Transform convention). Duan's analytical expression for S_ϕ then amounts to

$$S_\phi(\omega) = \frac{2Hk_BT^2(\beta + n\alpha)^2}{\lambda^2 r_0^4 \kappa} \int_1^\infty d\zeta' \int_1^\infty d\zeta \frac{e^{i\psi_0(\zeta-\zeta')}}{\zeta^2\zeta'^2} \int_0^R r^3 \exp\left[-\frac{r^2}{r_0^2}\left(\frac{1}{\zeta} + \frac{1}{\zeta'}\right)\right], \qquad (9)$$

where $\psi_0 = \omega r_0^2/(4D) = \pi f r_0^2/(2D)$ and $D = \kappa/C_p$. It turns out that an additional factor of 2 multiplies this S_ϕ expression because Duan's Fourier Transform only takes into account positive frequencies.

This integral was evaluated in Mathematica due to numerical noise in MATLAB's calculation. The calculation in Mathematica was very slow, so the upper limits on ζ and ζ' were often truncated, but an infinite upper limit is possible, as suggested in figure 3.

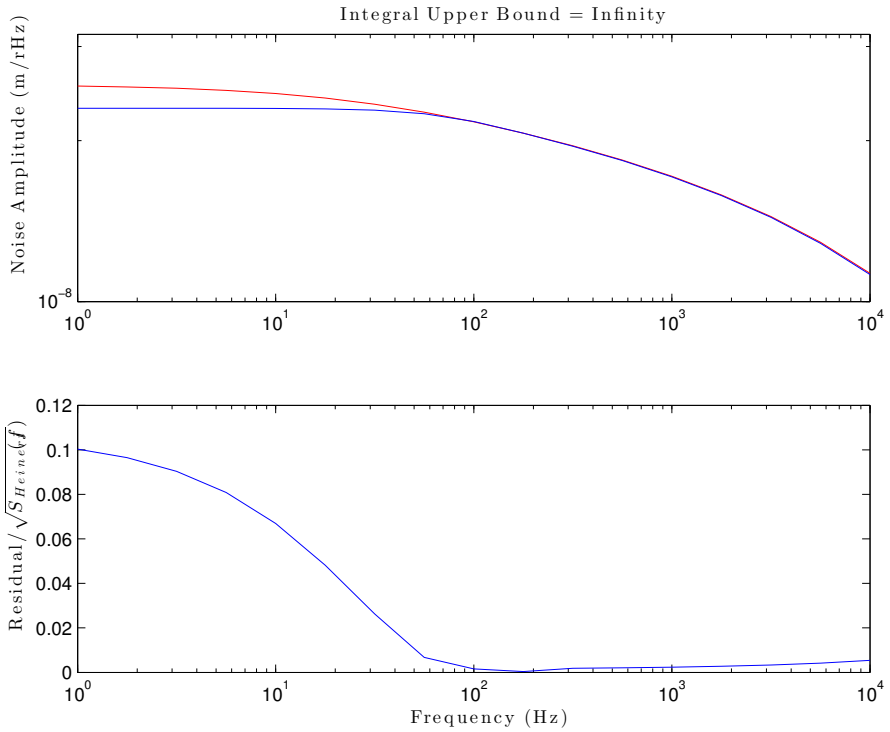

Figure 3: There is a maximum disagreement of 10 percent between the Heinert (blue) and Duan (red) curves, which occurs at the low frequency regime. Such a discrepancy has been attributed to lack of experimental investigation into this regime. The relevant parameters for equations 9 and 6 can be found in section V of the Duan paper.

There is a disagreement between the Duan and Heinert models at low frequencies. Still, the COMSOL model maintains the best agreement with the Heinert model. Using the Duan parameters given in section V of the paper, the TE, TR, and TO noises were calculated (all of which are scalar multiples of $S_T(f)$), producing figure 4.

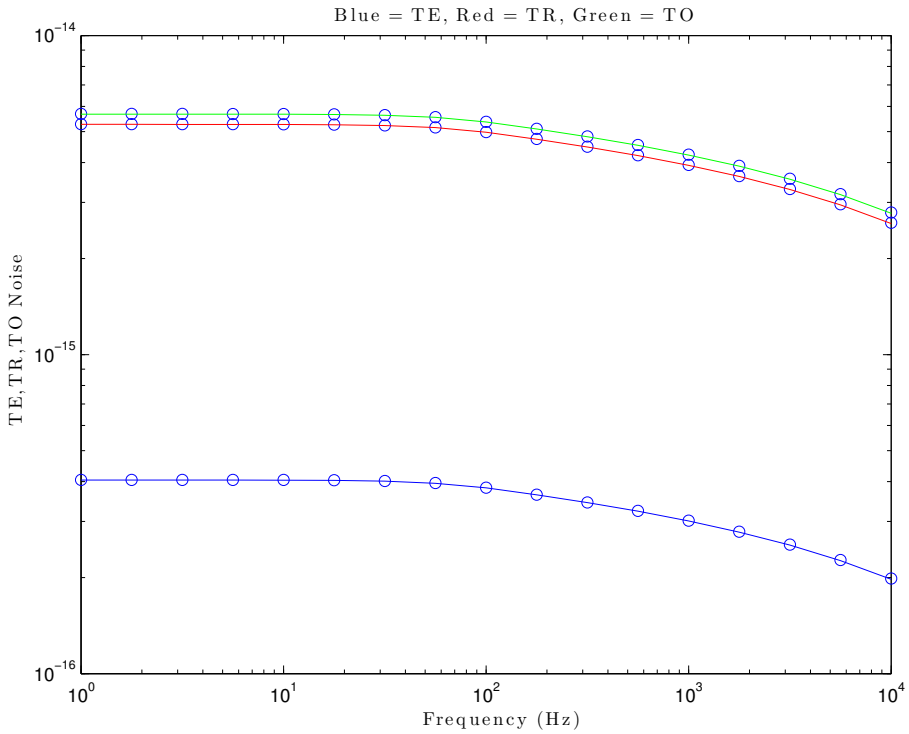

Figure 4: Noise spectrum for the Duan parameters. The TO spectrum is greater than the TE and TR spectrum because α and β are both positive. The solid line represents the Heinert Calculation, while the points represent the COMSOL FEA calculation.

The agreement obtained between the COMSOL model and Heinert's solution lend credence to (1) our steady-state approach of solving the heat equation (eq. 5) and (2) Heinert's analytical solution in eq. 6.

4.2 TIR Cavity

The previous section gave credence to our steady-state approach in thermal noise calculations. We therefore use the same method for thermal noise in the TIR cavity. The geometry in this case is a rectangular slab of width, length, and height W, L and H, respectively. A laser beam is injected through the center of the slab. That laser, undergoing total internal reflection, is assumed to not lose energy and that it reflects off of the center of the cavity walls. With this setup, the goal is to find a material that minimizes thermo-optic noise. Last year, some cancellation was observed for Sapphire at 300 K, using cylindrical test masses and the negative of its usual thermal expansion coefficient. In this case, it was found that the noises were correlated, which meant that cancellation of the noises was possible.

We assume, as a first approximation, that the laser consists of four gaussian beams of the form $e^{-(z^2+x'^2)/r_0^2}$, where x' denotes the horizontal distance from the beam's propagation axis, and z denotes the height. Interference effects at the reflection points are ignored, as are any

waists associated with the laser. For TR noise, then, we find that

$$q(\vec{r}) = Ae^{-z^2/r_0^2}[\exp[-(x\sin\theta - (y+L/2)\cos\theta)^2/r_0^2] + \exp[-((x-W/2)\sin\theta + y\cos\theta)^2/r_0^2] + \exp[-((x+W/2)\sin\theta - y\cos\theta)^2/r_0^2] + \exp[-(x\sin\theta + (y+L/2)\cos\theta)^2/r_0^2]] \quad (10)$$

is the heat injection that takes the form of the laser, where $\theta = \tan^{-1}(L/W)$. Also, recall that $A \equiv \beta T_0 F_0/(\pi r_0^2)$.

To calculate the thermal noise, COMSOL must solve equation 5 with this new heat injection. Adiabatic boundary conditions are assumed. The current work has been on establishing a reliable mesh size for this rectangular TIR cavity. We have created different meshing methods, from a uniform, 'extra fine', mesh to finely-meshed cylinders in the shape of the laser beam, surrounded by a coarser mesh. At this point, it is still unclear which mesh is the best, but the most promising appears to be a uniform mesh. Some different meshings of the TIR cavity are shown in figure 5.

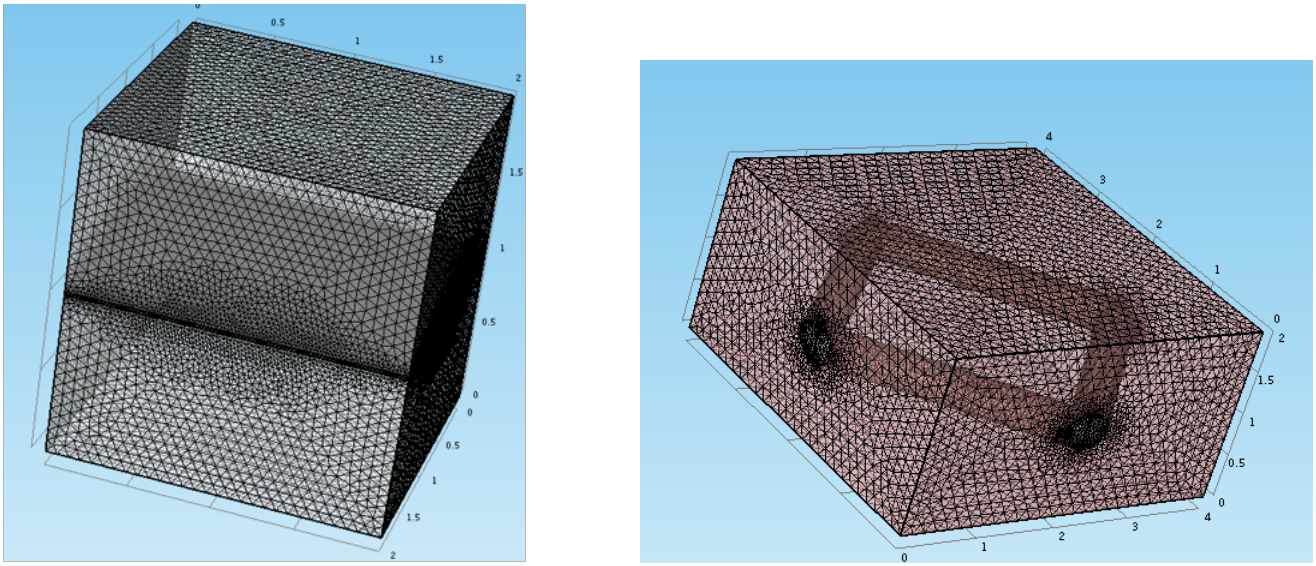

Figure 5: Screenshot from COMSOL, showing a 'sandwich' meshing (left) and a cylinder meshing (right). So far, it is unclear which mesh is the best, but comparison with an analytical model could help resolve this issue.

One way to find an ideal mesh is to compare the mesh's noise result with an analytical calculation. Consider a rectangular slab whose origin is at the center. The x, y, and z lengths are W, L, and H, respectively. For adiabatic boundary conditions, we therefore require

$$(\nabla T)_x|_{x=\pm\frac{W}{2}} = (\nabla T)_y|_{y=\pm\frac{L}{2}} = (\nabla T)_z|_{z=\pm\frac{H}{2}} = 0 \quad (11)$$

for the temperature field, which satisfies the steady-state heat equation (eq. 5) where q is the heat injection. In the absence of a heat injection, we know that T can be written as a Fourier series. Hence, we seek a solution of the form

$$T(\vec{r}) = \sum_{lmn} a_{lmn}\cos(r_l x)\cos(r_m y)\cos(r_n z) + b_{lmn}\sin(s_l x)\sin(s_m y)\sin(s_n z) \quad (12)$$

We will use the Fourier expansion of $q(\vec{r})$ to determine a_{lmm} and b_{lmm}. The z-dependence of q should be emphasized here: a Gaussian e^{-z^2/r_0^2}, where r_0 is the beam radius. This is an even function, which means that we only need to keep the cosine terms in the expansion for $T(\vec{r})$. In other words, $b_{lmn} = 0$. Since

$$\nabla T = -\sum_{lmn} a_{lmn}[r_l \sin(r_l x)\cos(r_m y)\cos(r_n z), \\ r_m \cos(r_l x)\sin(r_m y)\cos(r_n z), r_n \cos(r_l x)\cos(r_m x)\sin(r_n x)], \tag{13}$$

the boundary conditions (eqs. 11) give us

$$\frac{r_l W}{2} = l\pi, \quad \frac{r_m L}{2} = m\pi, \quad \frac{r_n H}{2} = n\pi \tag{14}$$

where l, m, n are integers. If we make them even integers, then we can write

$$T(\vec{r}) = \sum_{\text{even}} a_{lmn} \cos\left(\frac{l\pi x}{W}\right)\cos\left(\frac{m\pi y}{L}\right)\cos\left(\frac{n\pi z}{H}\right) \tag{15}$$

Our goal is to calculate to $S_z(\omega)$, which means we need to calculate the dissipation in eq. 4. Using the orthogonality relation

$$\int_{-W/2}^{W/2} \cos\left(\frac{l\pi x}{W}\right)\cos\left(\frac{l'\pi x}{W}\right) dx = \frac{W}{2}\delta_{ll'} \tag{16}$$

we then obtain

$$W_{\text{diss}} = \frac{\kappa\pi^2 V}{16 T_0}\sum_{\text{even}} |a_{lmn}|^2 \left(\frac{l^2}{W^2} + \frac{m^2}{L^2} + \frac{n^2}{H^2}\right) \tag{17}$$

where $V = WLH$. This gives, using eq. 1,

$$S_z(\omega) = \frac{8k_B T_0}{\omega^2}\frac{W_{\text{diss}}}{F_0^2} = \frac{\kappa k_B \pi^2 V}{2\omega^2 F_0^2}\sum_{\text{even}} |a_{lmn}|^2 \left(\frac{l^2}{W^2} + \frac{m^2}{L^2} + \frac{n^2}{H^2}\right) \tag{18}$$

Now we wish to determine a_{lmn}. To do this, we plug $T(\vec{r})$ into equation 5 and expand $q(\vec{r})$ as

$$q(\vec{r}) = \sum_{\text{even}} c_{lmn} \cos\left(\frac{l\pi x}{W}\right)\cos\left(\frac{m\pi y}{L}\right)\cos\left(\frac{n\pi z}{H}\right), \tag{19}$$

which means that

$$c_{lmn} = \frac{8}{V}\int q(\vec{r}) \cos\left(\frac{l\pi x}{W}\right)\cos\left(\frac{m\pi y}{L}\right)\cos\left(\frac{n\pi z}{H}\right) dV \tag{20}$$

Equation 5 then gives

$$i\omega c_{lmn} = a_{lmn}\left[i\omega C_p + \kappa\left(\frac{l^2\pi^2}{W^2} + \frac{m^2\pi^2}{L^2} + \frac{n^2\pi^2}{H^2}\right)\right] \tag{21}$$

or,

$$|a_{lmn}|^2 = \frac{c_{lmn}^2}{C_p^2 + \frac{\kappa^2\pi^4}{\omega^2}\left(\frac{l^2}{W^2} + \frac{m^2}{L^2} + \frac{n^2}{H^2}\right)^2} \tag{22}$$

Plugging this into equation 18, we find that

$$S_z(\omega) = \frac{\kappa k_B \pi^2 V}{2F_0^2} \sum_{\text{even}} \frac{|c_{lmn}|^2}{C_p^2 \omega^2 \left(\frac{l^2}{W^2} + \frac{m^2}{L^2} + \frac{n^2}{H^2}\right)^{-1} + \kappa^2 \pi^4 \left(\frac{l^2}{W^2} + \frac{m^2}{L^2} + \frac{n^2}{H^2}\right)} \tag{23}$$

For convenience, let $d_{lmn} = c_{lmn}/A$. Then

$$S_z(\omega) = \frac{\kappa k_B T_0^2 \beta^2 V}{2r_0^4} \sum_{\text{even}} \frac{|d_{lmn}|^2}{C_p^2 \omega^2 \left(\frac{l^2}{W^2} + \frac{m^2}{L^2} + \frac{n^2}{H^2}\right)^{-1} + \kappa^2 \pi^4 \left(\frac{l^2}{W^2} + \frac{m^2}{L^2} + \frac{n^2}{H^2}\right)} \tag{24}$$

We considered the following parameters: $L = W = H = 4$ cm, $T = 120$ K, $r_0 = 1$ mm, $\beta = 8.7 \times 10^{-5}$ K^{-1}, $C_p/\rho = 328$ J/kg/K, $\rho = 2331$ kg/m^3, and $\kappa = 615$ W/m/K. Given these parameters, the Fourier coefficients were be plotted to determine the proper cutoff indices in the triple sum of equation 24 . Note that the heat injection can be written in the form $q(\vec{r}) = q(z)q(x, y)$. This separation of variables means that we can write $d_{lmn} = d_n d_{lm}$, where d_n is the z-component of the Fourier coefficient, and d_{lm} is the xy component of the Fourier series. These coefficients are shown in figure 6. They suggest that we can truncate the series at $n = 50$ and $l = m = 30$.

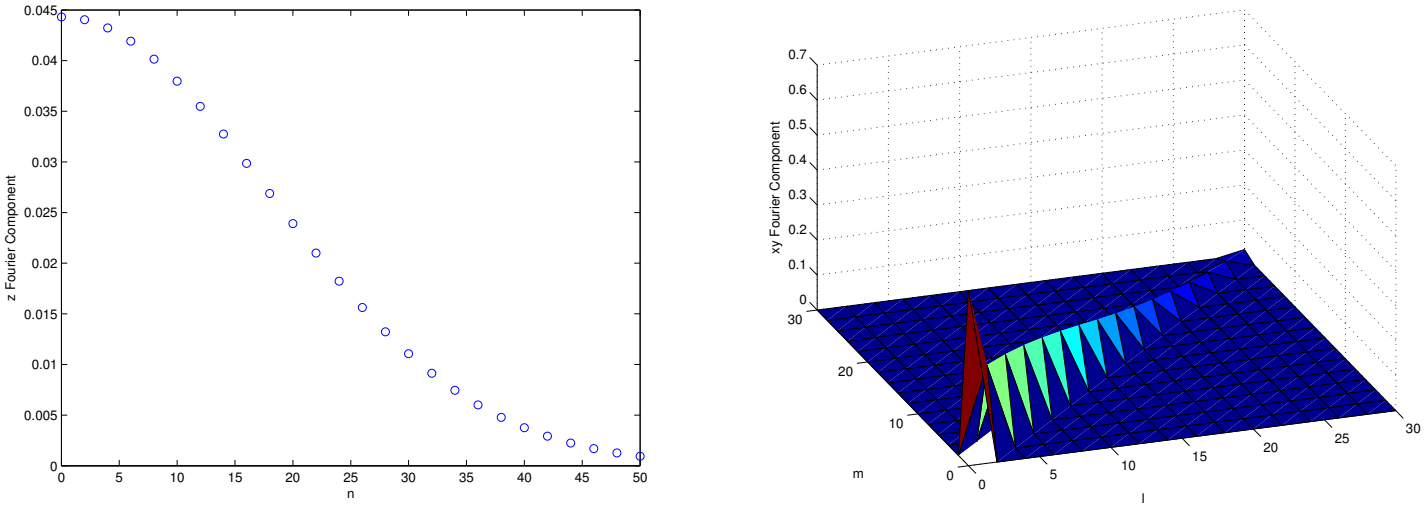

Figure 6: The z-component should go out to about 50 terms, while the xy components should go out to about 30 terms. Moreover, the diagonal $m = l$ only contributes to the Fourier series, allowing us to neglect many terms.

By contrast, a beam size of $r_0 = 0.1$ mm requires many more terms, as indicated in figure 7. This makes sense for the following the reason. The Fourier series terms have an effective wavelength which go as L/m. For an accurate solution, we need to resolve down to the smallest length scales, which means that $m_{\max}$ satisfies $L/m_{\max} \sim r_0$. Hence, if $L \sim 10^{-2}$ m and $r_0 \sim 10^{-4}$ m, then $m_{\max} \sim 10^2$.

Taking these plots into account, we can have more confidence in the accuracy of the analytical Fourier Series solution. The analytical solution in equation 24 therefore gives a tool for assessing the accuracy of the numerical solution. The next plot (figure 8) compares this

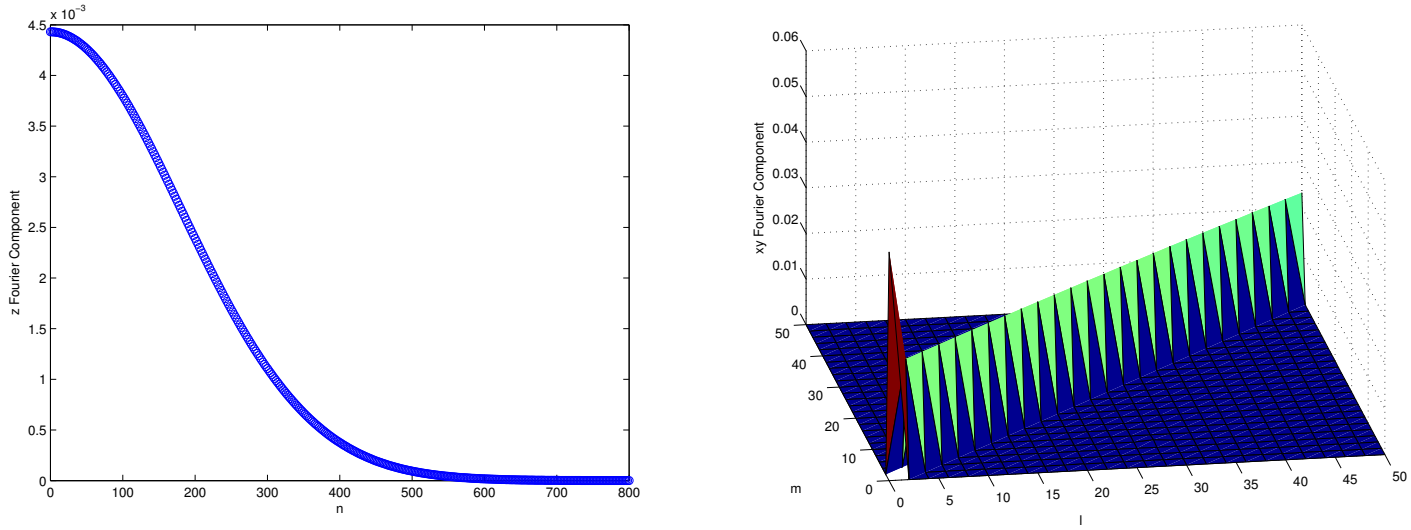

Figure 7: A smaller beam size requires more terms before the Fourier Series converges.

solution with COMSOL. With more confidence in the analytical solution's accuracy, we can more likely attribute error to the meshing. At the moment, it appears that a uniform meshing is giving the closest agreement to the analytical model.

The differences between the analytical and numerical solutions are likely attributed to meshing inaccuracies In COMSOL, the mesh size runs from 0.008 to 0.11 cm. Meanwhile, the smallest length scale is the thermal wavelength $r_{\rm th} = \sqrt{\kappa/(C_p\omega)} \sim 10^{-2}$ cm for a frequency of 10^4 Hz. The mesh size is often larger than this, indicating that meshing could be an issue at high frequencies. Furthermore, a beam size of 1 mm may also yield some meshing difficulties, since that is slightly below the maximum mesh size.

The following is a tentative time frame for the remainder of the project.

1. Verify the best mesh for the TIR cavity.

2. Calculate the TE noise for the rectangular cavity. We suspect that to apply the Levin approach here, we need to apply an oscillating force to both the inside (via a heat injection) and the outside (via a strain distribution).

3. Explore the parameter space (time permitting). Find the optimum parameter set that reduces thermal noise. Upon calculating the thermal noise, the goal is to find a material where this noise is minimized. The goal is to achieve cancellation of these two coefficients by finding the right material. If such a material can be found, the goal will be to build a setup for laser stabilization with that material. This could help identify unknown sources of noise.

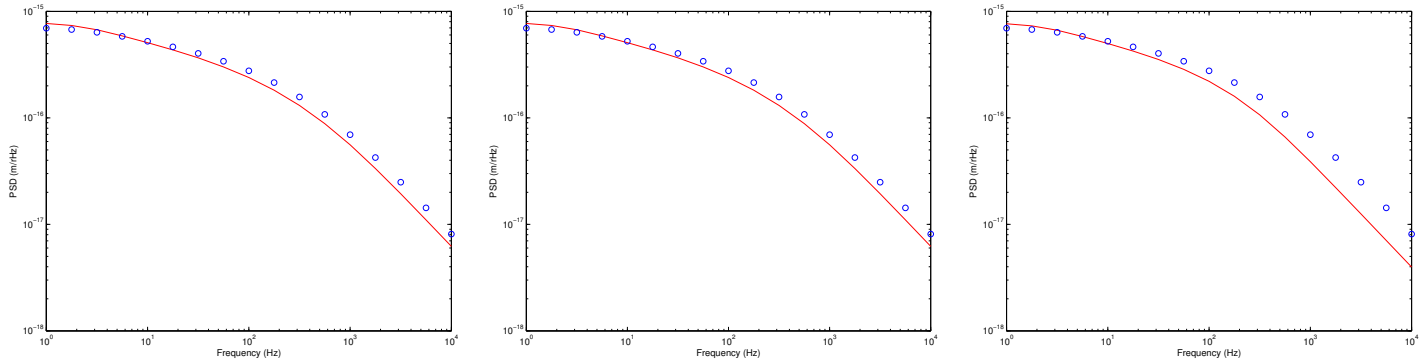

Figure 8: Equation 24 was used to calculate the analytical plot of $\sqrt{S_z(f)}$ (red), truncating the sum at $n = 60$ and $l = m = 40$ on the left, $n = 50$, $m = l = 30$ in the middle (the minimum required from figure 6), $n = 20$ and $l = m = 10$ on the right. Moreover, only $l = m$ terms were included in the sum. The blue numerical solutions (same for all) is given a uniform, finer mesh. So far, this uniform mesh gives the best observed agreement with the analytical model.

References

[1] Schiller, et al. *Fused-silica monolithic total-internal-reflection resonator.* Optics Letters (1991).

[2] Evans, et. al., *Thermo-optic noise in coated mirrors for high-precision optical measurements.* Physical Review D78, 102003 (2008).

[3] Chatterjee, Deep, *Design of a coating-less reference cavity with total internal reflection.* LIGO Report. (2013).

[4] Levin, Y. (1998). *Internal thermal noise in the LIGO test masses: A direct approach.* Physical Review D, 57(2), 659

[5] Heinert, et al. *Thermorefractive noise of finite-sized cylindrical test masses.* Physical Review D84, 062001 (2011).

[6] Duan, Lingze. *General treatment of the thermal noise in optical fibers.* Physical Review A86, 023717 (2012).